Electronic Supplementary Material (ESI) for Catalysis Science & Technology.
This journal is © The Royal Society of Chemistry 2020

ELECTRONIC SUPPLIMENTARY INFORMATION

Novel $La(OH)_3$ Integrated sGO-Ag_3VO_4/Ag Nanocomposite as a Heterogeneous Photocatalyst for Fast Degradation of Agricultural and Industrial Pollutants

Ragam N. Priyanka, Subi Joseph, Thomas Abraham, Neena J. Plathanam, and Beena Mathew*

*School of Chemical Sciences, Mahatma Gandhi University, Kottayam-686560, Kerala, India. *Email:* beenamscs@gmail.com

Characterization of sGO

sGO is characterized by various techniques as shown below.

a) Fourier Transform Infra-Red spectroscopy

In the FT-IR spectrum of GO, vibrations from oxygen functionalities are clear from the peaks at 3267, 1720, 1160, and 1039 cm^{-1} representing –OH, -C=O, C-OH and –C-O-C- stretching respectively. But in sGO, the intensity of those peaks are considerably minimized pointing to a major removal of oxygen containing functional groups. Thus, peaks corresponding to –OH and C-OH bonds were absent in sGO while C=O peak is present with lower intensity in sGO at 1741 cm^{-1}. The peak of C-O-C stretching is totally disappeared owing to the possible removal of epoxides from GO, forming C-S-C bonds, denoted by peak at 1210 cm^{-1}. In addition, peak at 1370 cm^{-1} can be assigned as S=O from sGO [1]. These observations lead to the successful doping of sulfur atoms to GO sheet [2].

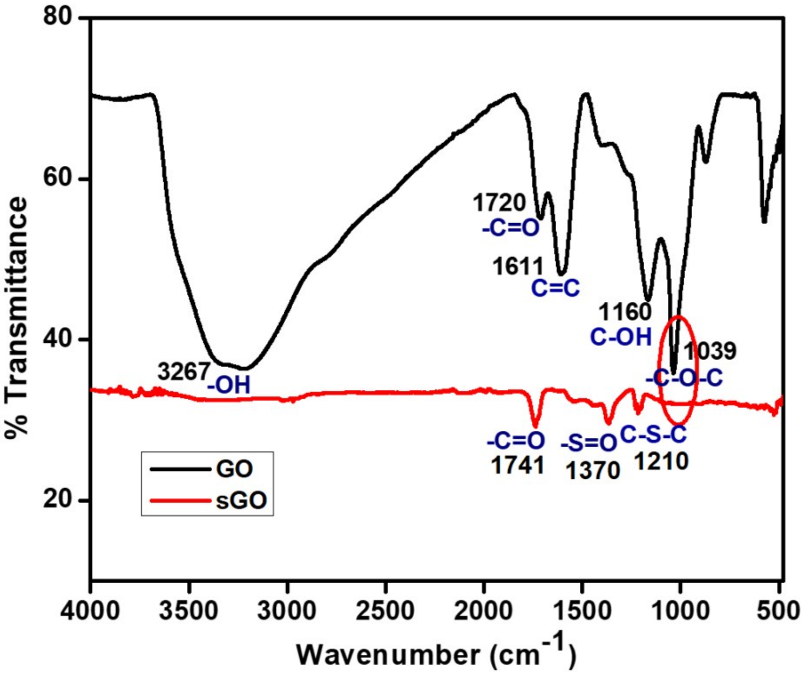

Fig. S1a: FT-IR spectra of GO and sGO

b) UV-visible Diffuse Reflectance Spectroscopy

Comparison of UV-vis. DRS spectra of GO and sGO convey that the sulfur doping lead to an increment in absorption intensity as well as improved absorption in visible region, extending to the near-IR region [3].

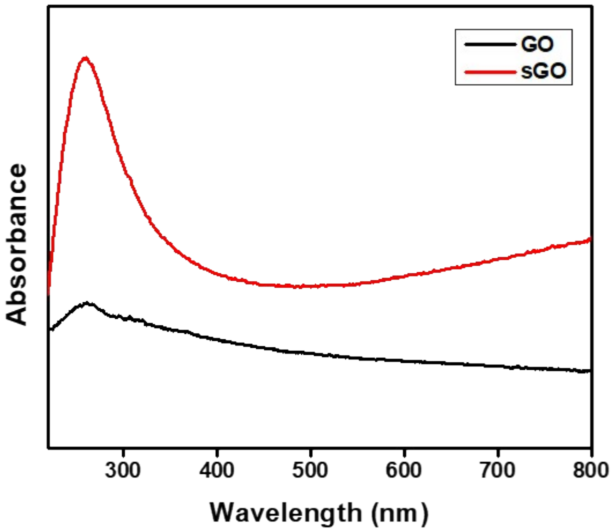

Fig. S1b: UV-vis. DRS spectra of GO and sGO

c) Photoluminescence spectroscopy

The emission intensity of sGO was found very much reduced than GO from photoluminescence spectra. This indicates a minimalized recombination of charges in sGO compared to GO, which can be due to the higher conductivity of sGO [4].

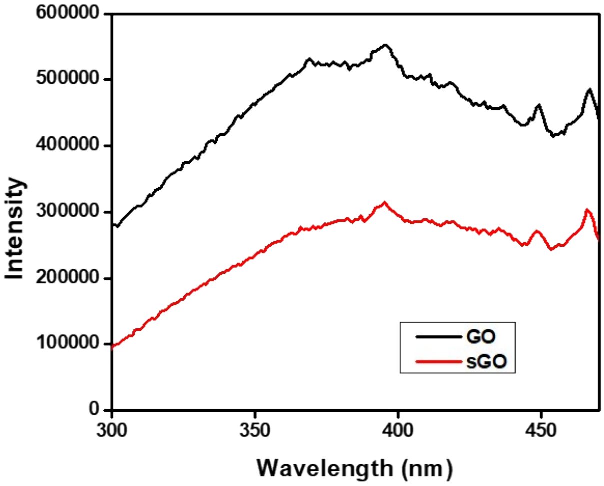

Fig. S1c: PL spectra of GO and sGO

d) X-Ray Diffraction analysis

The XRD peaks at 24.01° and 43.49° represent (002) and (100) planes of sGO [5, 6]. These peaks are absent in GO which has only a single peak at 11° from (001) peak [6].

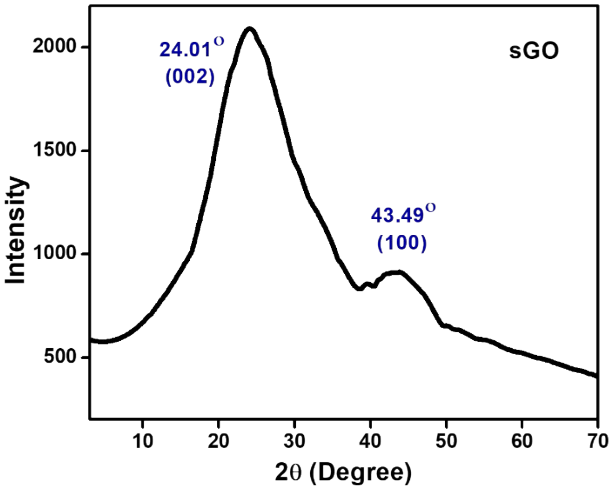

Fig. S1d: XRD spectrum of sGO

e) X-ray Photoelectron Spectroscopy analysis

Survey XPS spectrum of sGO represented peaks at 166, 230, 285 and 531 eV representing S2p, S2s, C1s and O1s, respectively. XPS spectrum of S2p span from 162-172 eV. The spectrum displayed peak at 166.51 eV which can be assigned to C-S-C groups of sGO [7].

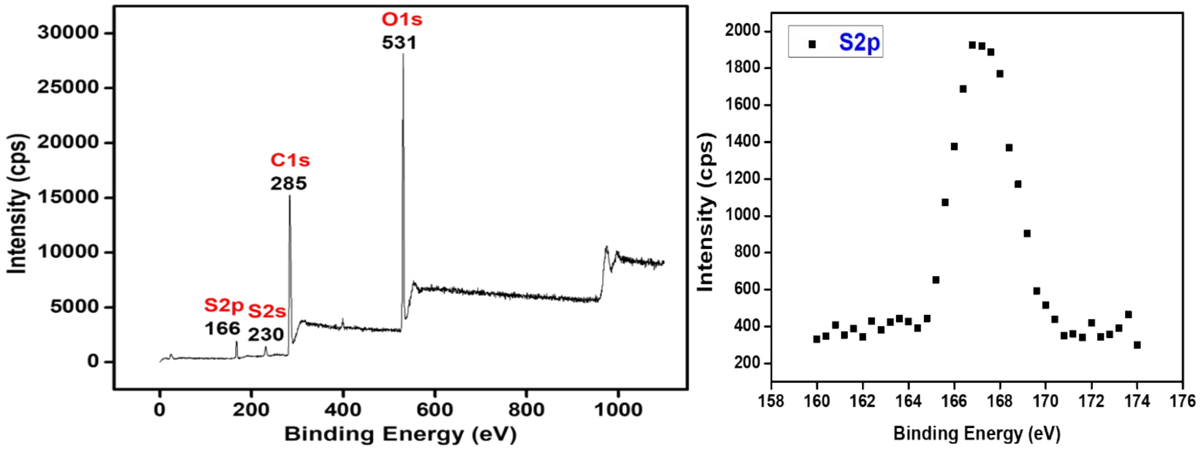

Fig. S1e: Survey and S2p XPS spectra of sGO

f) Scanning Electron Microscopy analysis

The SEM image of sGO clearly shows the presence of sheet like structure.

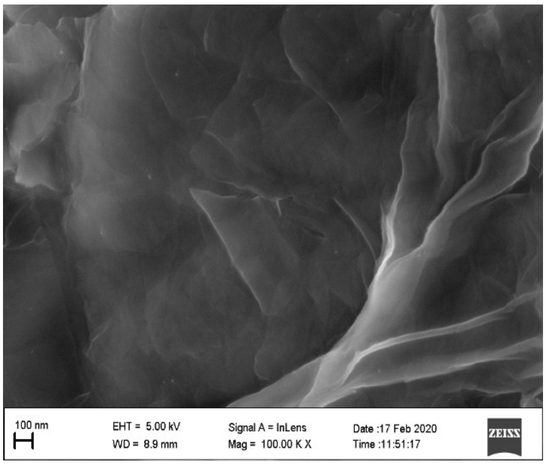

Fig. S1f: FESEM image of sGO

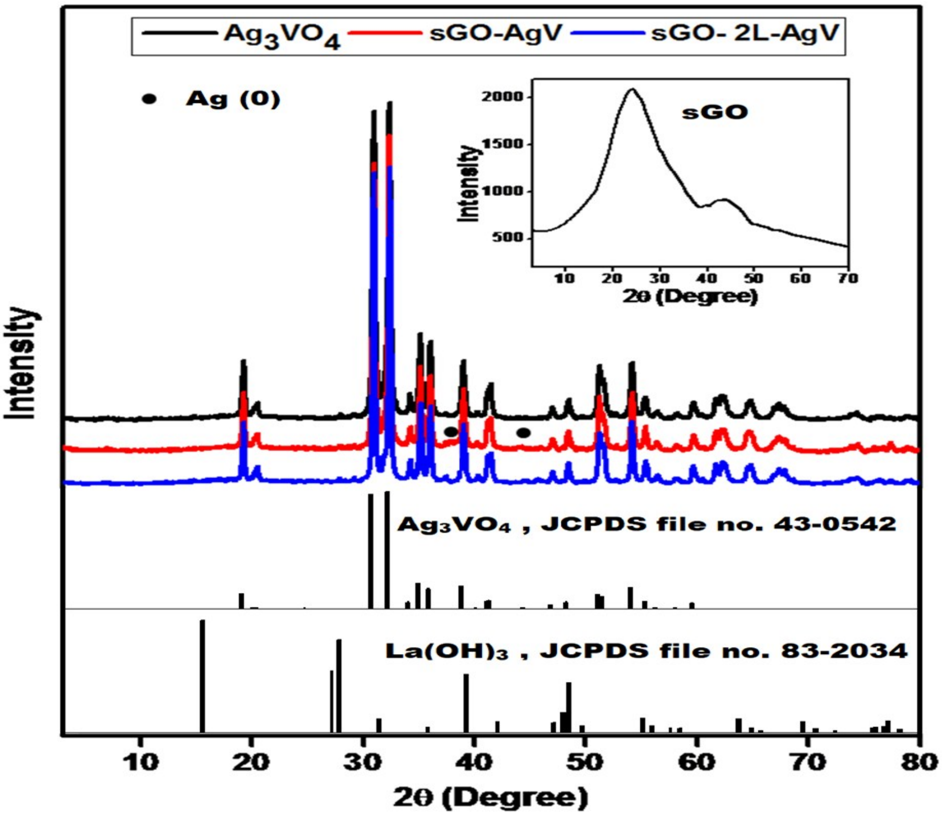

Fig. S2: XRD of composites compared with standard XRD of La(OH)$_3$

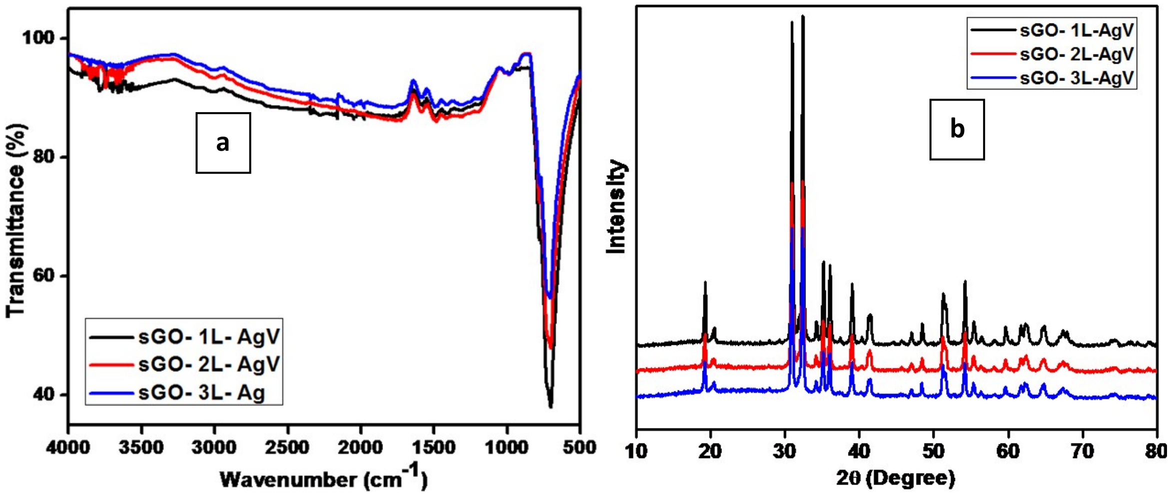

Fig. S3: (a) FT-IR and (b) XRD spectra of 1 %, 2% and 3% $La(OH)_3$ modified 1% sGO-Ag_3VO_4/Ag catalysts

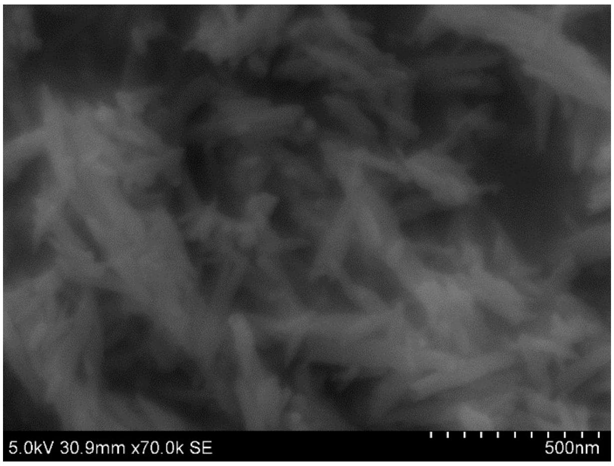

Fig. S4: SEM image of $La(OH)_3$

BET surface area analysis of composites

Results of BET analysis of composites are provided below. Compared to the precursor, the novel composite sGO-2L-AgV displayed improved surface area as can be seen from the table.

Table S1: Surface area of composites.

Sample	BET Surface area (m^2/g)
sGO-AgV	8.30
sGO-2L-AgV	10.66

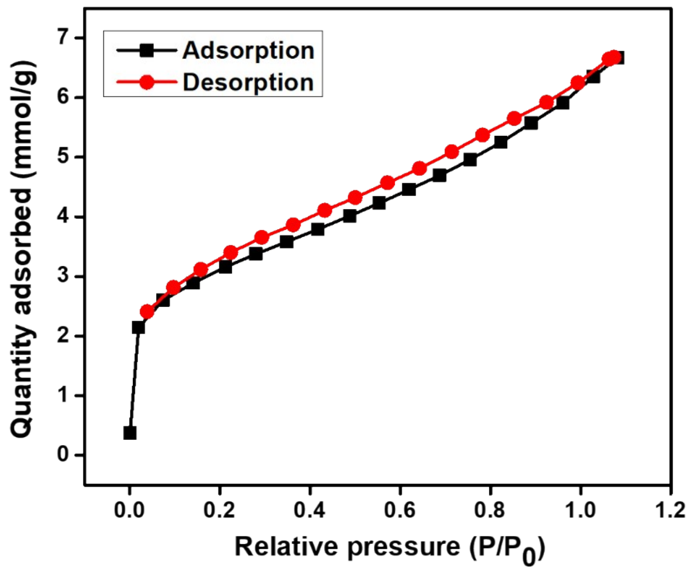

Fig. S5: BET adsorption–desorption isotherm of the sGO-2L-AgV

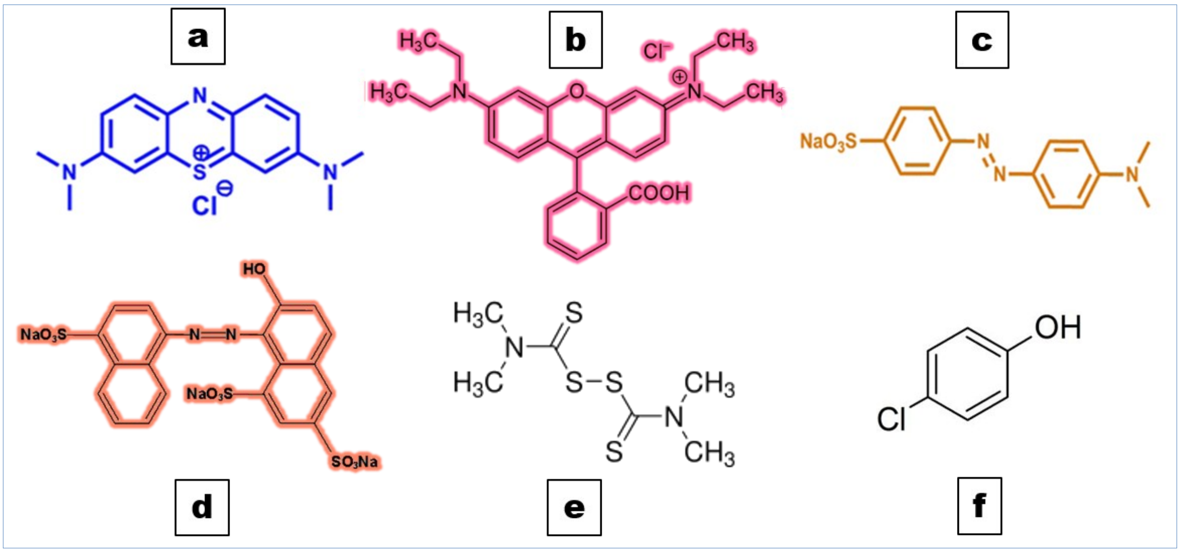

Fig. S6: Structures of (a) methylene blue, (b) rhodamine B, (c) methyl orange, (d) acid red 18, (e) thiram and (f) 4-chlorophenol

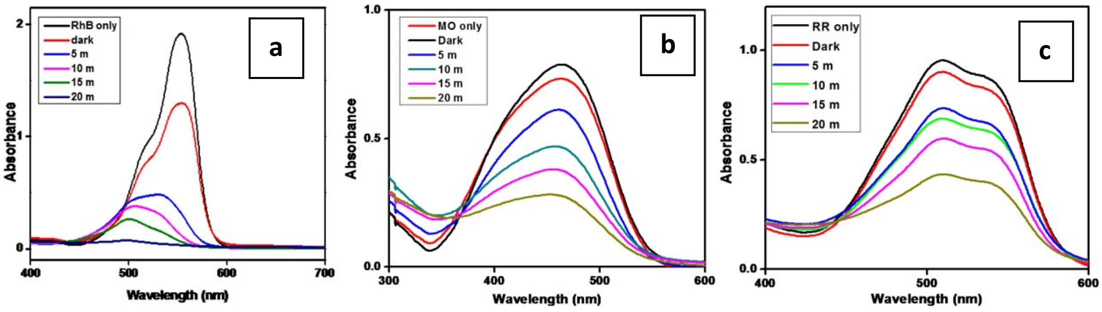

Fig. S7: Degradation of (a) Rhodamine B, (b) Methyl Orange, and (c) Acid Red 18 by sGO-2L-AgV

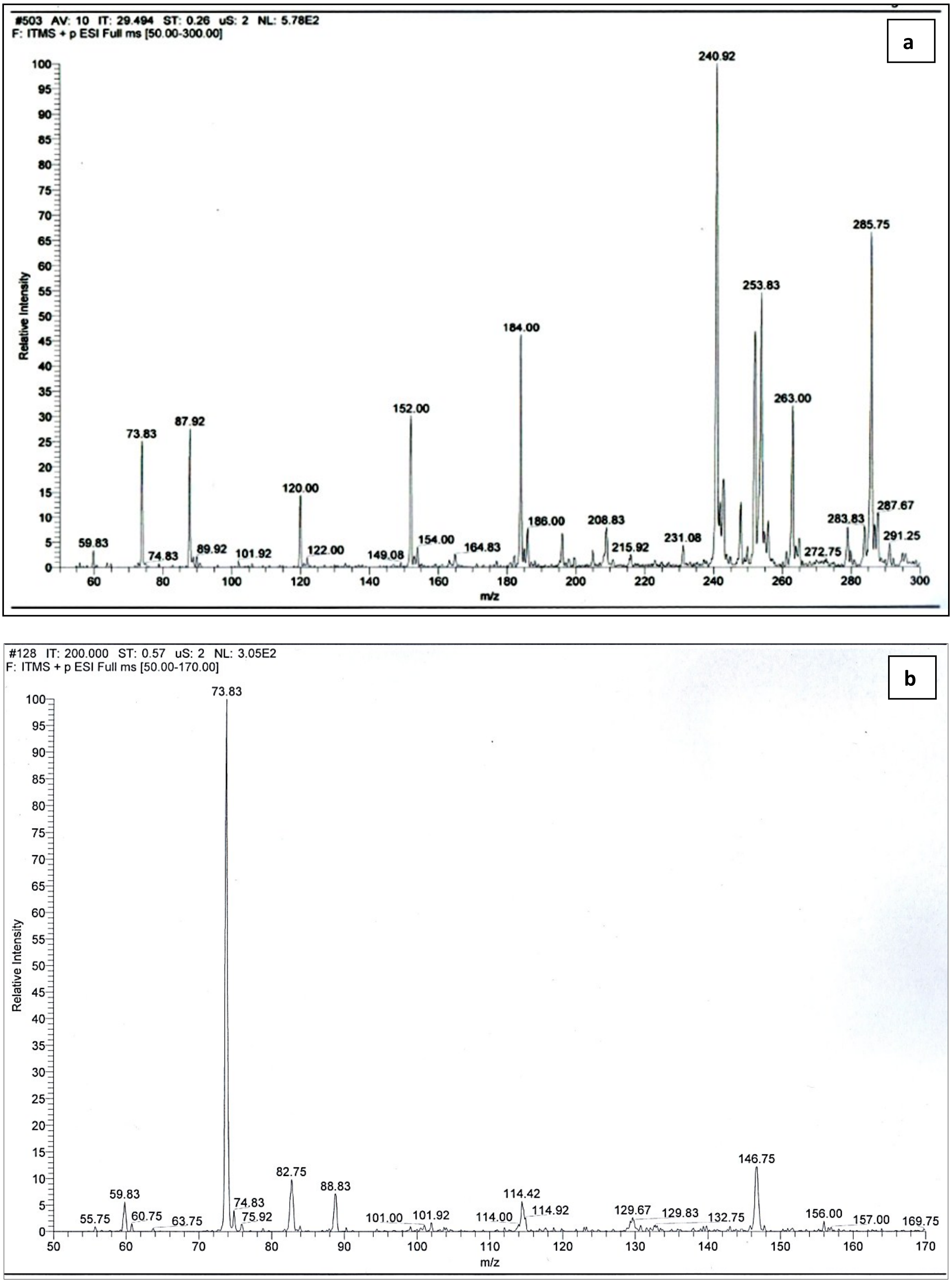

Fig. S8: Mass spectra of thiram, (a) pure and (b) after 2 h photocatalytic degradation

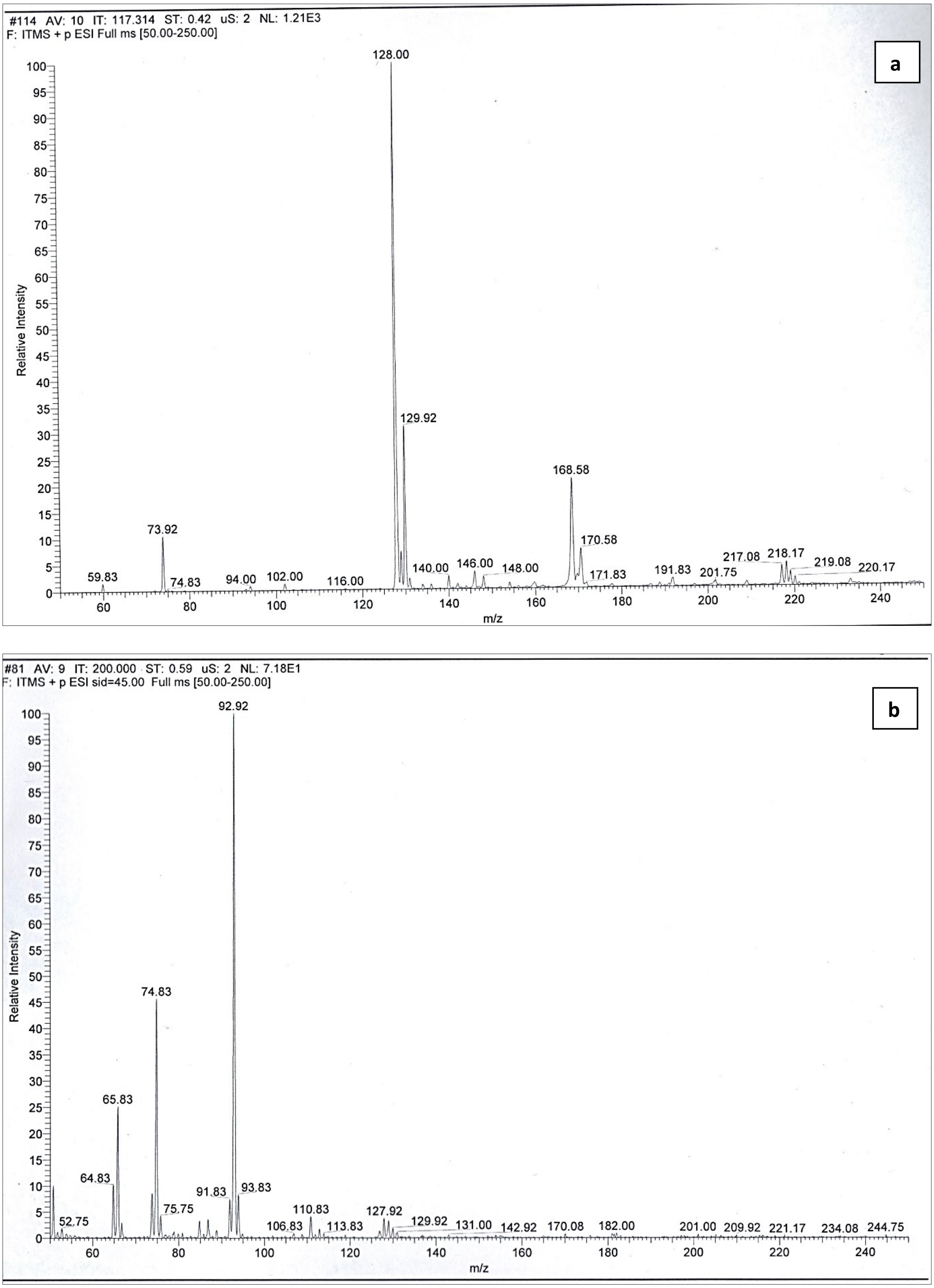

Fig. S9: Mass spectra of 4-chlorophenol, (a) pure and (b) after 3 h photocatalytic degradation

Table S2: Rate constants and degradation (%) of methylene blue by various catalysts

Catalysts	Rate constant, k (min^{-1})	Degradation in 15 minutes (%)
sGO	0.001	4.66
Ag_3VO_4	0.047	31.97
sGO-AgV	0.109	85.30
sGO- 1L- AgV	0.138	89.14
sGO- 2L- AgV	0.307	99.92
sGO- 3L- AgV	0.196	95.95

Table S3: Total organic carbon (TOC) content removal of dyes (after 1 h), thiram (after 2 h) and 4-chlorophenol (after 3 h) using sGO-2L-AgV photocatalyst

Pollutant	TOC removal (%)
Methylene blue	98
Rhodamine B	96
Methyl orange	73
Acid Red 18	70
Thiram	81
4-chlorophenol	78

Table S4: Comparison of pollutant degradation by sGO-2L-AgV with literature

Catalyst	Light source	Pollutant removal (%)	References
Ag/$AgVO_3$/BiOCl, 50 mg BiOCl, 50 mg Ag/$AgVO_3$, 50 mg	Visible light Xenon lamp (300 W), 14 V, 16 A	Methylene Blue, 100 mL (7 mg/L), 93.16% (t=60 min) 29.24% 37.52%	[8]
g-C_3N_4/Fe_3O_4/Ag_3VO_4, 0.1 g	Visible light LED source (50 W)	Rhodamine B, 250 ml, (t=240 min)	[9]
ZnO/Ag_3VO_4/Fe_3O_4/0.1 g	Visible light LED source (50 W)	Rhodamine B, 250 ml (1x10^{-5} M), (t=240 min)	[10]
Ag_3VO_4/Bi_2WO_6, 35 mg	Visible light (λ=400 nm)	Rhodamine B, 100 ml (10 mg/L), 91.4% (t>60 min)	[11]
Fe_3O_4/ZnO/Ag_3VO_4/AgI, 0.1 g	Sunlight	Rhodamine B, 250 ml (1x10^{-5} M), ~95% (t=70 min)	[12]
Rb_xWO_3/Ag_3VO_4, 10 mg	Visible light Xenon lamp (500 W),	Rhodamine B (10 mg/L), 92 % (t=120 min)	[13]

	400-780 nm	Methylene blue, 93% (t=60 min)	
$Ag_3VO_4/Zn_3(VO_4)_2/Zn_2V_2O_7/ZnO$, 30 mg	Sunlight	Rhodamine B (10 ppm), 94.95% (t=60 min) Methyl orange (10 ppm), 49.74% (t=300 min) Orange II (10 ppm), 77.84% (t=60 min) Methylene Blue (20 ppm), 93.89% (t=25 min)	[14]
Ag_3VO_4@MIL-125-NH_2, 100 mg	LED visible light, 12 W	Rhodamine B, 100 ml (5 mg/L), t> 50 min	[15]
1% sGO-Ag_3VO_4/Ag, 50 mg	Sunlight, flux = 960 W/m^2	Methylene Blue, 100 ml (10 mg/L) 97% (t=30 min), Rhodamine B 100 ml (10 mg/L) 95% (t=30 min), Methyl Orange 100 ml (10 mg/L) 60% (t=30 min), Acid Red 18 100 ml (10 mg/L) 49% (t=30 min), Thiram, 100 ml (20 mg/L) 100% (t=60 min)	[16]
1% sGO-2% $La(OH)_3$-Ag_3VO_4/Ag, 50 mg	Sunlight, flux = 960 W/m^2	Methylene Blue, 100 ml (10 mg/L) 99.95% (t=20 min), Rhodamine B 100 ml (10 mg/L) 97.70% (t=20 min), Methyl Orange 100 ml (10 mg/L) 62.37% (t=20 min), Acid Red 18 100 ml (10 mg/L) 51.68% (t=20 min), Thiram, 100 ml (20 mg/L) 100% (t=60 min) 4-chlorophenol, 100 ml (20 mg/L) 100% (t=180 min)	This work

Band Potentials of Ag_3VO_4 and $La(OH)_3$

For a semiconducting material, its valence band potential can be calculated from the following equation,

$$E_{VB} = \chi - E_C + 0.5\,Eg$$

In the equation, X denotes the absolute electronegativity of semiconductor, EC represents the energy of free electrons on the hydrogen scale which is ~4.5 eV and Eg is the bandgap energy. The value of χ is 5.64 eV for Ag_3VO_4 and the value of Eg obtained from the Tauc plot is 2.14 eV. Thus, from the equation, the valence band potential for Ag_3VO_4 was found as 2.21 eV. The conduction band potential can be found out from the following equation [17],

$$E_{CB} = E_{VB} - Eg$$

Thus, 0.07 eV was found as the conduction band potential of Ag_3VO_4.

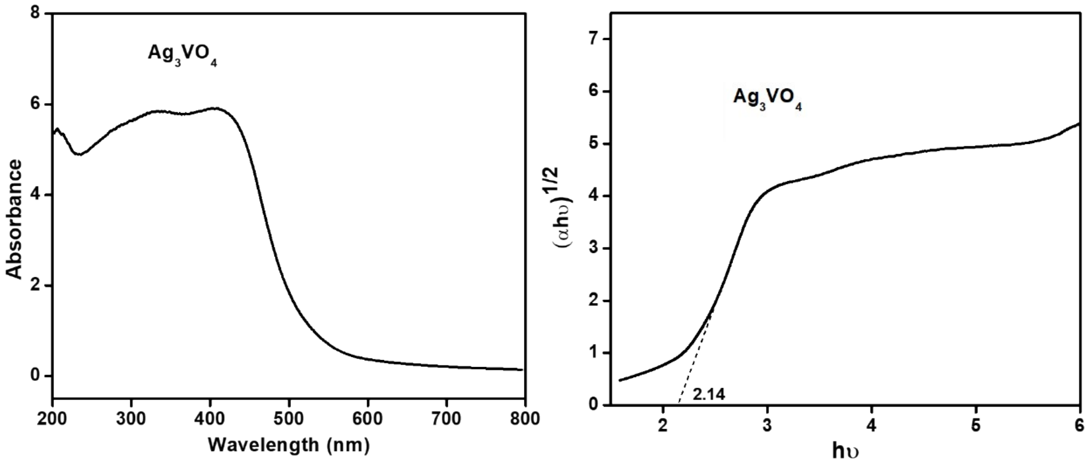

Fig. S10: UV-vis. DRS spectrum and Tauc plot of Ag_3VO_4

Similarly, for $La(OH)_3$, χ is 5.67 eV and Eg found from the Tauc plot is 4.82 eV. Thus as per the previous calculations, VB and CB obtained are 3.58 and -1.24 eV, respectively which are comparable to previous reports [18].

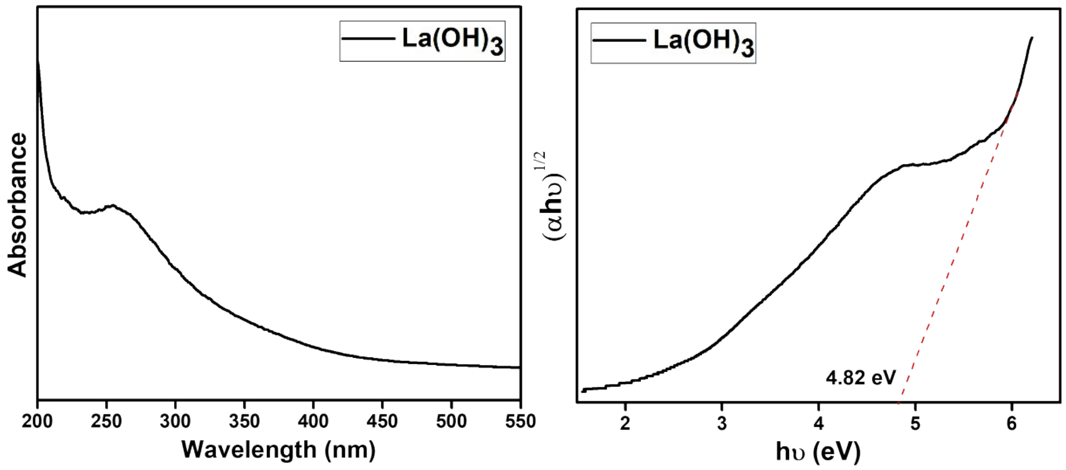

Fig. S11: UV-vis. DRS spectrum and Tauc plot of $La(OH)_3$

References

[1] J. Gliniak, J.-H. Lin, Y.-T. Chen, C.-R. Li, E. Jokar, C.-H. Chang, C.-S. Peng, J.-N. Lin, W.-H. Lien, H.-M. Tsai, and T.-K. Wu, “Sulfur-doped graphene oxide quantum dots as photocatalysts for hydrogen generation in the aqueous phase,” ChemSusChem, 2017, 10, 3260.

[2] N. Karikalan, R. Karthik, S.-M. Chen, C. Karuppiah, and A. Elangovan, “Sonochemical synthesis of sulfur doped reduced graphene oxide supported CuS nanoparticles for the non-enzymatic glucose sensor applications,” Scientific Reports, 2017, 7, 1.

[3] S. Joseph, S. Abraham, T. Abraham, R. N. Priyanka, and B. Mathew, “S-rGO modified sulphur doped carbon nitride with mixed-dimensional hierarchical nanostructures of silver vanadate for the enhanced photocatalytic degradation of pollutants in divergent fields,” Applied Surface Science, 2019, 495, 143478.

[4] Y. Tian, Y. Liu, W. Wang, X. Zhang, and W. Peng, “Sulfur-doped graphene-supported Ag nanoparticles for nonenzymatic hydrogen peroxide detection,” Journal of Nanoparticle Research, 2015, 17, 1.

[5] T. Wang, L.-X. Wang, D.-L. Wu, W. Xia, and D.-Z. Jia, “Interaction between nitrogen and sulfur in co-doped graphene and synergetic effect in supercapacitor,” Scientific Reports, 2015, 5, 1.

[6] W. Han, L. Chen, W. Song, S. Wang, X. Fan, Y. Li, F. Zhang, G. Zhang, and W. Peng, “Synthesis of nitrogen and sulfur co-doped reduced graphene oxide as efficient metal-free cocatalyst for the photo-activity enhancement of CdS,” Applied Catalysis B: Environmental, 2018, 236, 212.

[7] X. Chen, X. Chen, X. Xu, Z. Yang, Z. Liu, L. Zhang, X. Xu, Y. Chen, and S. Huang, “Sulfur-doped porous reduced graphene oxide hollow nanosphere frameworks as metal-free electrocatalysts for oxygen reduction reaction and as supercapacitor electrode materials,” Nanoscale, 2014, 6, 13740.

[8] L. Zhang, X. Yuan, H. Wang, X. Chen, Z. Wu, Y. Liu, S. Gu, Q. Jiang, and G. Zeng, “Facile preparation of an Ag/$AgVO_3$/BiOCl composite and its enhanced photocatalytic behavior for methylene blue degradation.” RSC Advances, 2015, 5, 98184.

[9] M. Mousavi and A. Habibi-Yangjeh, “Ternary g-C_3N_4/Fe_3O_4/Ag_3VO_4 Nanocomposites: Novel Magnetically Separable Visible-Light-Driven

Photocatalysts for Efficiently Degradation of Dye Pollutants.” Materials Chemistry and Physics, 2015, 163, 421.

[10] M. Shekofteh-Gohari and A. Habibi-Yangjeh, “Ternary ZnO/Ag_3VO_4/Fe_3O_4 nanocomposites: novel magnetically separable photocatalyst for efficiently degradation of dye pollutants under visible-light irradiation.” Solid State Sciences, 2015, 48, 177.

[11] S. Li, S. Hu, W. Jiang, Y. Liu, J. Liu, and Z. Wang, “Facile synthesis of flower-like Ag_3VO_4/Bi_2WO_6 heterojunction with enhanced visible-light photocatalytic activity.” *Journal of Colloid and Interface Science,* 2017, 501, 156.

[12] Habibi-Yangjeh and M. Shekofteh-Gohari, “Novel magnetically separable Fe_3O_4 @ZnO/AgCl nanocomposites with highly enhanced photocatalytic activities under visible-light irradiation.” Separation and Purification Technology, 2015, 147, 194.

[13] T. F. Chala, C.-M. Wu, and K. G. Motora, C. Yu, D. Zeng, F. Chen, H. Ji, J. Zeng, D. Li, and K. Yang, “RbxWO_3/Ag_3VO_4 Nanocomposites as efficient full-spectrum (UV, visible, and near-infrared) photocatalysis.” Journal of the Taiwan Institute of Chemical Engineers, 2019, 102, 465.

[14] C. Yu, D. Zeng, F. Chen, H. Ji, J. Zeng, D. Li, and K. Yang, “Construction of efficient solar-light-driven quaternary Ag_3VO_4/$Zn_3(VO_4)_2$/$Zn_2V_2O_7$/ZnO heterostructures for removing organic pollutants via phase transformation and in-situ precipitation route.” Applied Catalysis A: General, 2019, 578, 70.

[15] H. E. Emam, H. B. Ahmed, E. Gomaa, M. H. Helal, and R. M. Abdelhameed, “Doping of silver vanadate and silver tungstate nanoparticles for enhancement the photocatalytic activity of MIL-125-NH_2 in dye degradation.” Journal of Photochemistry and Photobiology A: Chemistry, 2019, 383, 111986.

[16] R. N. Priyanka, S. Joseph, T. Abraham, N. J. Plathanam, and B. Mathew, “Rapid sunlight-driven mineralisation of dyes and fungicide in water by novel sulphur-doped graphene oxide/Ag_3VO_4 nanocomposite,” Environmental Science and Pollution Research, Jan. 2020, doi:10.1007/s11356-019-07569-7.

[17] W. Li, Q. Chen, X. Lei, and S. Gong, “Fabrication of Ag/AgBr/Ag_3VO_4 composites with high visible light photocatalytic performance,” RSC Advances, 2019, 9, 5100.

[18] F. Dong, X. Xiao, G. Jiang, Y. Zhang, W. Cui, and J. Ma, “Surface oxygen-vacancy induced photocatalytic activity of $La(OH)_3$ nanorods prepared by a fast and scalable method,” Physical Chemistry Chemical Physics, 2015, 17, 16058.